Dye Laser Photolysis of *n*-Pentanal from 280 to 330 nm

Thomas J. Cronin and Lei Zhu*

Wadsworth Center, New York State Department of Health, Department of Environmental Health and Toxicology, State University of New York, Albany, New York 12201-0509

Received: June 4, 1998; In Final Form: September 14, 1998

The UV photolysis of *n*-pentanal in the 280−330-nm region has been studied in 5-nm intervals by using dye laser photolysis in combination with cavity ring-down spectroscopy. Absorption cross sections of *n*-pentanal were measured at each wavelength studied. *n*-Pentanal exhibited a broad, structureless absorption band similar, in appearance, to that of previously studied short-chain aldehydes. The absorption spectrum peaked at 295 nm with a cross section of $(6.56 \pm 0.17) \times 10^{-20}$ cm^2 molecule^{-1}. The formation of the HCO radical, which is a photodissociation product, was monitored in these experiments. The HCO yield was found to be independent of *n*-pentanal pressure (2−18 Torr) and total pressure (8−480 Torr) except for 325- and 330-nm photolysis where the size of the HCO signal was small and the dissociation was near the threshold. The dependence of the HCO radical yield on the photolysis wavelength was determined. The HCO yields were 0.058 ± 0.006, 0.095 ± 0.009, 0.10 ± 0.02, 0.14 ± 0.01, 0.10 ± 0.02, 0.15 ± 0.02, 0.14 ± 0.02, 0.20 ± 0.06, 0.14 ± 0.02, 0.085 ± 0.034, 0.087 ± 0.015 at 280, 285, 290, 295, 300, 305, 310, 315, 320, 325, and 330 nm, respectively, where uncertainty reflects experimental scatter only. End products from closed-cell photolysis of *n*-pentanal with and without O_2 were investigated at 290, 310, and 330 nm by using GC/MS and HPLC. Acetaldehyde was found to be a significant product from the photodissociation of *n*-pentanal/N_2 mixtures. Photolysis rates of *n*-pentanal to form HCO were calculated for two representative atmospheric conditions (noontime at sea level and 40° N latitude on January 1 and on July 1). The estimated radical formation rate constants from *n*-pentanal photolysis were about twice as fast as those obtained from acetaldehyde photolysis.

Introduction

Aldehydes play an important role in the formation of photochemical smog, peroxyacetyl nitrate (PAN), and regional ozone. Photodissociation of aldehydes represents a significant source of free radicals in the lower atmosphere.[1−3] There have been a relatively large number of studies devoted to the photodissociation of shorter chain aldehydes, such as CH_2O, CH_3CHO, and C_2H_5CHO.[4−12] However, the photolysis of longer chain aldehydes is not well-understood. Such an investigation is important in order to determine the fates of longer chain aldehydes in the atmosphere and to understand their contribution to radical formation.

Aliphatic aldehydes exhibit a weak absorption band in the wavelength range 240−360 nm as a result of a dipole forbidden $n \rightarrow \pi^*$ transition.[13,14] Photolysis of *n*-pentanal can possibly occur through the following pathways:

$$CH_3(CH_2)_3CHO + h\nu \rightarrow C_4H_{10} + CO \qquad \Delta H^\circ_{298} = -7.8 \text{ kJ·mol}^{-1} \quad (1)$$

$$\rightarrow n\text{-}C_4H_9 + HCO \qquad \Delta H^\circ_{298} = 348.3 \text{ kJ·mol}^{-1} \quad (2)$$
$$(\lambda \leq 343 \text{ nm})$$

$$\rightarrow C_4H_9CO + H \qquad \Delta H^\circ_{298} = 365.7 \text{ kJ·mol}^{-1} \quad (3)$$
$$(\lambda \leq 327 \text{ nm})$$

$$\rightarrow CH_3CH{=}CH_2 + CH_3CHO \qquad \Delta H^\circ_{298} = 82.2 \text{ kJ·mol}^{-1} \quad (4)$$
$$(\lambda \leq 1454 \text{ nm})$$

where photochemical thresholds were calculated from the corresponding enthalpy changes. In the absence of experimental heats of formation for *n*-C_4H_9 and C_4H_9CO, enthalpy changes for channels (2) and (3) were assumed to be the same as those for the photolysis of propionaldehyde. This assumption is reasonable since channel (2) involves the breaking of a methylene carbonyl bond (−CH_2−CHO) and channel (3) involves the breaking of a carbonyl hydrogen bond (−C(O)−H) from photolysis of both propionaldehyde and *n*-pentanal.

In this paper, we report results obtained from the dye laser photolysis of *n*-pentanal in the wavelength region 280−330 nm. Absorption cross sections of *n*-pentanal were measured. The HCO radical yield from the photolysis of *n*-pentanal was determined by using a sensitive new detection technique, cavity ring-down spectroscopy.[15,16] The absolute HCO concentrations were calibrated relative to those obtained from the photolysis of formaldehyde (H_2CO) at each wavelength. We have also investigated products from closed-cell photolysis of *n*-pentanal with and without oxygen at 290, 310, and 330 nm by using GC/MS and HPLC.

Experimental Section

The apparatus, which has been described in detail elsewhere,[17,18] was modified by the addition of a Lambda Physik Scanmate II dye laser and a second-harmonic generation unit which were placed downstream from the excimer laser that pumped them. The fundamental of an excimer-pumped dye laser can produce tunable pulsed output from 330 nm to 1.05 μm. Frequency doubling of the fundamental dye laser output allows wavelength tunability in the 220−330-nm range. It was the addition of a dye laser and a frequency doubler that enabled continuous tuning of the photolysis wavelength. The second-harmonic crystal used in the present experiments was a KDP

10.1021/jp982487s CCC: $15.00
Published on Web 11/17/1998

crystal. The following laser dyes were used to cover the spectral range 280−330 nm: Coumarin 153, Rhodamine 6G, Rhodamine B, Rhodamine 101, Sulforhodamine 101, and DCM.

The dye laser pumped by a 308-nm XeCl excimer (∼180 mJ/pulse) produced an energy output of ∼20 mJ/pulse (typical dye efficiency is 8−14% depending upon the laser dyes used). Frequency doubling of the fundamental output of the dye laser yielded ∼2 mJ of useable UV light for photolysis. Further losses along the optical path to the photolysis cell reduced the actual useable energy to less than 2 mJ/pulse. The photodissociation dye laser pulse entered the reaction cell at a 15° angle with the main cell axis through a sidearm and overlapped the probe beam at the center of the cavity. The probe laser pulse from a nitrogen-pumped dye laser was directed along the main optical axis of the cell vacuum-sealed with a pair of high reflectance (∼99.999% at 614 nm) cavity mirrors. A fraction of the probe laser output was transmitted into the cavity through the front mirror. The photon intensity decay inside the cavity was measured from the weak transmission of light through the rear mirror with a photomultiplier tube (PMT). The PMT output was amplified, digitized, and sent to a computer. The decay curve was fit to a single-exponential decay function from which the total loss per optical pass was calculated. Sample absorption was determined by measuring cavity losses in the presence and absence of resonant absorption. Absorption spectra were recorded by scanning the wavelength of the probe laser with a digital drive unit. The photolysis laser pulse energy was measured with a calibrated Joule meter.

Gas pressures at the center of the reaction cell were measured with a Baratron capacitance manometer. *n*-Pentanal pressure used in the experiments ranged from 2 to 18 Torr. All measurements except spectral scans were carried out at a laser repetition rate of 0.1 Hz to ensure replenishment of the gas sample between successive laser shots. Spectrum scans were performed at a repetition rate of 1 Hz. All experiments were conducted at room temperature which was 293 ± 2 K.

n-Pentanal is a liquid at room temperature and was obtained from Aldrich Chemical Co. (∼99% purity) Impurities in *n*-pentanal included ≤0.07% *n*-butyraldehyde and 1% *n*-pentanoic acid. Effects of these impurities on the accuracy of cross section and HCO yield measurements will be discussed in the following section. *n*-Pentanal vapor was used in the experiments. It was purified by repeated freeze−pump−thaw cycles and stored under vacuum. Formaldehyde was generated by the pyrolysis of polymer paraformaldehyde (Aldrich Chemical Co.; ≥95% purity) at 110 °C. Nitrogen (≥99.999% purity, UHP grade) and oxygen (≥99.994% purity, UHP grade) were purchased from MG Industries and were used without further purification.

Results and Discussion

Absorption Cross Sections of *n*-Pentanal in the 280−330-nm Region. Depicted in Figure 1 are room-temperature absorption cross sections of $C_5H_{10}O$ as a function of wavelength in the 280−330-nm range. The absorption cross section at each wavelength was obtained by measuring the transmitted photolysis photon intensity as a function of *n*-pentanal pressure in the cell and by applying the Beer−Lambert relation to the data obtained. Error bars quoted (1σ) on Figure 1 are the estimated precisions of cross section determinations which includes the standard deviation for each measurement (∼0.5%) plus the standard deviation about the mean of at least four repeated experimental runs. Besides random errors, systematic errors also contribute to the uncertainty in cross section values. The major sources of systematic errors are those involving pressure (0.1%) and path length (0.2%) determinations, and other systematic errors from the presence of impurity (∼1%) in *n*-pentanal. Since *n*-pentanoic acid only absorbs UV radiation shorter than 260 nm,[13] the presence of 1% *n*-pentanoic acid in *n*-pentanal will systematically lower the values of the absorption cross sections by 1%. Absorption cross sections of *n*-butyraldehyde[19] are about 5% smaller than those of *n*-pentanal in the wavelength range studied. As a result, the presence of ≤0.07% *n*-butyraldehyde would decrease *n*-pentanal cross section values by ≤0.0035%. Adding relative (see Table 1) and systematic errors, the overall uncertainty for *n*-pentanal cross section measurements is 5% in the 280−325-nm range, and 16% at 330 nm. Included in Figure 1 for comparison are previously reported absorption spectra of C_2-C_4 aldehydes.[19] As can be seen, the spectral shape of *n*-pentanal is similar to those reported previously for C_2-C_4 aldehydes. Cross section data (in units of cm^2 molecule^{-1}, base e) obtained from this study are also tabulated in Table 1.

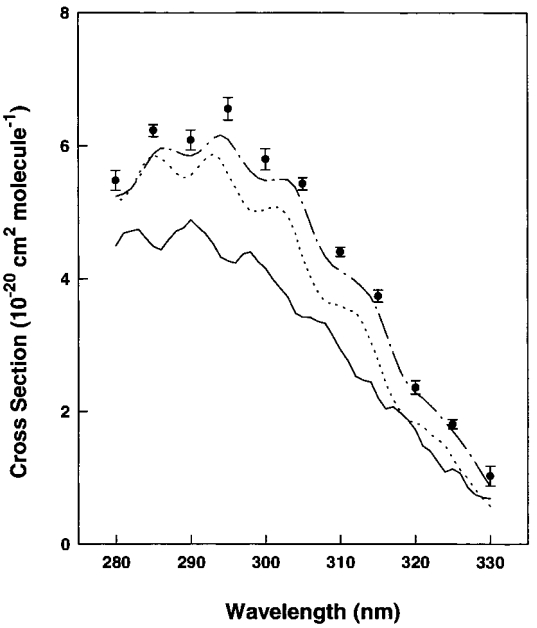

Figure 1. Absorption cross sections in the 280−330-nm region at room temperature. This work on *n*-pentanal (●) and previous determinations of C_2-C_4 aldehyde cross sections by Martinez et al.: acetaldehyde (solid line), propionaldehyde (dashed line), and *n*-butyraldehyde (dotted line).

TABLE 1: Absorption Cross Sections and HCO Radical Yields of *n*-Pentanal as a Function of Wavelength

λ (nm)	σ (10^{-20} cm^2 molecule^{-1})	φ(HCO)
280	5.48 ± 0.15	0.058 ± 0.006
285	6.23 ± 0.09	0.095 ± 0.009
290	6.09 ± 0.15	0.10 ± 0.02
295	6.56 ± 0.17	0.14 ± 0.01
300	5.80 ± 0.16	0.10 ± 0.02
305	5.43 ± 0.09	0.15 ± 0.02
310	4.41 ± 0.07	0.14 ± 0.02
315	3.74 ± 0.09	0.20 ± 0.06
320	2.36 ± 0.10	0.14 ± 0.02
325	1.81 ± 0.07	0.085 ± 0.034
330	1.03 ± 0.15	0.087 ± 0.015

HCO Quantum Yield from Photolysis of *n*-Pentanal in the 280−330-nm Range. Shown in Figure 2 is a ring-down absorption spectrum of the product from 290-nm photolysis of *n*-pentanal measured at a photolysis/probe laser delay of 15 μs in the wavelength region 613−616 nm. The resemblance of the photoproduct absorption spectrum to the reported absorption spectrum[20−23] of HCO in the same spectral region indicates that

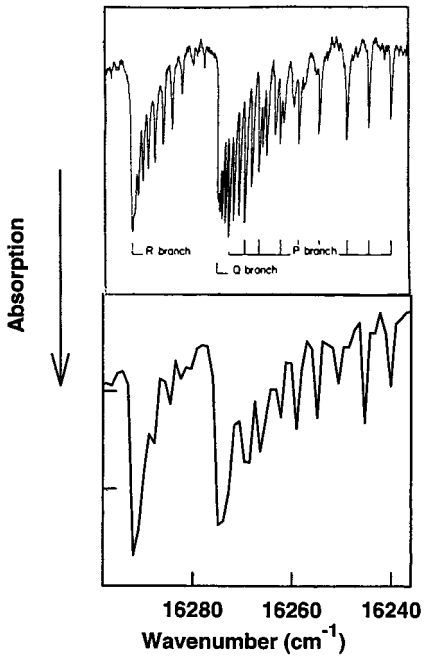

Figure 2. The lower trace is a low-resolution cavity ring-down absorption spectrum of the product following the photolysis of 4-Torr *n*-pentanal at 290 nm. The upper trace is a time-resolved intracavity laser absorption spectrum of the $(00^10) \rightarrow (09^00)$ vibronic transition of HCO following the 266-nm photolysis of 0.1-Torr CH_3CHO and 10-Torr Ar (adapted from ref 22).

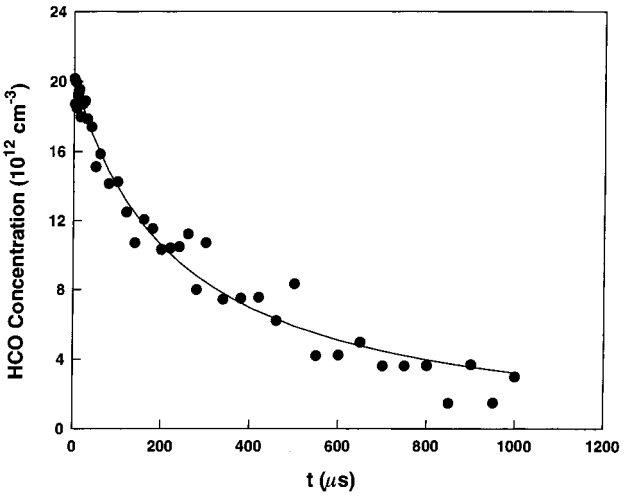

Figure 3. Typical time profile of the HCO radical. Photolysis at 290 nm of 4-Torr *n*-pentanal. Also shown is a fit to the kinetic model involving HCO + HCO, HCO + n-C_4H_9, and n-C_4H_9 + n-C_4H_9 reactions.

HCO is a photolysis product. The sharp absorption bands correspond to a vibronic transition from the vibrationless level of the ground state $^2A'$ (00^10) to the vibrationally and electronically excited $^2A''$ (09^00) state. The cavity ring-down spectrometer was tuned to a HCO absorption resonance at 613.8 nm (R bandhead), and the HCO concentration as a function of time was monitored. The time dependence of the HCO concentration was obtained by varying the delay time between the firing of the photolysis and the probe lasers and measuring the corresponding changes in absorption losses. Presented in Figure 3 is a typical time profile of the HCO radical along with a fit to the data. As seen from Figure 3, HCO appeared immediately after the 290-nm photolysis pulse and its concentration decayed as a function of time. Experimental studies of smaller aldehydes (RCHO) have shown that R + HCO is the only important radical formation channel around 300 nm.[13] Assuming that this channel is also the only important radical formation channel around 300 nm for *n*-pentanal, then the time dependence of HCO decay following photolysis can be modeled by the following kinetic scheme consisting of three coupled second-order equations:

$$HCO + HCO \rightarrow H_2CO + CO \quad (5)$$

$$HCO + C_4H_9 \rightarrow \text{products} \quad (6)$$

$$C_4H_9 + C_4H_9 \rightarrow C_8H_{18} \quad (7a)$$

$$\rightarrow C_4H_{10} + C_4H_8 \quad (7b)$$

To extract rate constants from HCO concentration decays, we compared time-resolved HCO decay profiles from the photolysis of 4-, 8-, and 16-Torr *n*-pentanal with those calculated using the ACUCHEM simulation program. Input parameters for the ACUCHEM program included initial estimates for $k_{HCO+HCO}$ and $k_{HCO+C_4H_9}$ (eqs 5 and 6, respectively) as well as input values for $k_{C_4H_9+C_4H_9}$ (eq 7) and HCO initial concentration ($[HCO]_0$). The simulated decay profile was compared with the experimental HCO decay profile, and then $k_{HCO+HCO}$ and $k_{HCO+C_4H_9}$ were adjusted until an optimum fit of experimental data was accomplished. A value of 2.0×10^{-12} cm^3 molecule^{-1} s^{-1} for $k_{C_4H_9+C_4H_9}$ was used in the fitting (rate constants of 1.9×10^{-12} cm^3 molecule^{-1} s^{-1} and 2.0×10^{-12} cm^3 molecule^{-1} s^{-1} were reported[24,25] for $C_2H_5 + C_2H_5$ and n-$C_3H_7 + n$-C_3H_7 reactions, respectively). An average of four experiments gave $k_{HCO+HCO}$ and $k_{HCO+C4H9}$ of $(7.3 \pm 1.7) \times 10^{-11}$ and $(6.5 \pm 1.5) \times 10^{-11}$ cm^3 molecule^{-1} s^{-1}, respectively. Errors are 1σ and represent experimental scatter only. Systematic errors such as uncertainties in the values of $[HCO]_0$, $k_{C_4H_9+C_4H_9}$, and time resolution of the cavity ring-down technique (ring-down time of $\sim$12 μs at the wavelength range studied) also contributed to overall uncertainty in the fitted values of $k_{HCO+HCO}$ and $k_{HCO+C_4H_9}$. We estimate systematic error because of the time resolution of the cavity ring-down technique to be a maximum of 5%. If we assume errors in the estimation of $[HCO]_0$ and $k_{C_4H_9+C_4H_9}$ to be 15% and 10%, respectively, then the overall error, including the experimental scatter in the fitted value of $k_{HCO+HCO}$ and $k_{HCO+C_4H_9}$, is $\sim$53%. The extracted $k_{HCO+HCO}$ and $k_{HCO+C_4H_9}$ rate constants are in good agreement with the recommended rate constant[26] for the HCO + HCO reaction ($k = 5.0 \times 10^{-11}$ cm^3 molecule^{-1} s^{-1} at 300 K; $\Delta \log k = \pm 0.3$) and the previously reported rate constants[24] for the HCO + C_2H_5 ($(7.2 \pm 1.6) \times 10^{-11}$ cm^3 molecule^{-1} s^{-1}) and HCO + n-C_3H_7 ($(6.5 \pm 1.3) \times 10^{-11}$ cm^3 molecule^{-1} s^{-1}) reactions.

Although HCO radicals were generated the whole length of the level arm through which the photolysis laser pulse traveled, the cavity ring-down technique only monitored HCO radical concentration in the region where the photolysis and probe laser beam overlapped. This region could be envisioned as a rectangular solid with width and height defined by those of the photolysis beam, and length defined by (beam width) $\times$ $\tan^{-1}$ (15°), where 15° is the angle between the photolysis beam and probe beam. The yield of HCO was derived from the ratio of the HCO concentration produced in this overlapping region to the absorbed photon density in the same region. Absorption of the photolysis beam by *n*-pentanal in the photolysis/probe laser overlapping region was calculated from the difference in the transmitted photolysis photon intensity at the beginning and at the end of the overlapping region. The incident light intensity was determined with a Joule meter, which was calibrated by acetone photolysis actinometry,[13] by measuring the photolysis

photon energy into the cell. To correct for photon transmission loss at the front window of the cell, photolysis photon intensity before and after an empty cell was determined. Transmission loss was ~8%/window. Once the absorption cross section of *n*-pentanal at a given photolysis wavelength and the light intensity incident onto *n*-pentanal were known, the absorbed photon density in the overlapping region of the photolysis and the probe lasers could be calculated for a given initial *n*-pentanal pressure. The HCO concentration produced at a given photolysis wavelength was obtained from lossmeter measurements of the HCO absorption intensity at 613.8 nm at a photolysis-to-probe laser delay of 15 μs. To convert HCO absorption losses into absolute concentrations, the absorption cross section of HCO at the probe laser wavelength needed to be known. The absorption cross section of HCO was determined in the present study relative to the photolysis reaction $H_2CO + h\nu \rightarrow HCO + H$, for which the HCO quantum yield is known.[26] Since H_2CO is easily polymerizable, it was produced immediately prior to each calibration run. The H_2CO sample purity was checked using FTIR; H_2O and CO_2 impurities were not observed. The purity of H_2CO was estimated by comparing the absorption cross section of H_2CO determined at each photolysis wavelength with literature values. The H_2CO absorption cross section was determined by measuring transmitted photolysis photon intensity as a function of H_2CO pressure in the cell and by applying the Beer−Lambert relation to the data obtained. Except for 290 and 310 nm, our H_2CO cross section data agreed within ±15% of those obtained by Moortgat et al.[4] at $\lambda \leq 300$ nm and by Cantrell et al.[27] in the 300−330-nm region. At 290 nm, an average of seven cross section measurements yielded an H_2CO cross section of $(6.98 \pm 1.04) \times 10^{-21}$ cm^2, which is 86% smaller than that of 1.30×10^{-20} cm^2 reported by Moorgat et al.[4] H_2CO exhibits a structured absorption spectrum in the 280−330-nm region. The cross section reported by Moorgat et al. was averaged over a 0.5-nm interval. Our photolysis laser has a wavelength resolution of 0.15 cm^{-1}. If there were a dip in the H_2CO absorption spectrum, it would be reflected in the cross section value obtained. Cantrell et al.[27] reported absorption cross sections of 2.22×10^{-20} cm^2 and 9.31×10^{-21} cm^2 at 308.75 and 311.25 nm, respectively. Their extrapolated cross section at 310 nm is 1.58×10^{-20} cm^2, which is 70% higher than our value of $(9.25 \pm 1.70) \times 10^{-21}$ cm^2. Since cross sections changed dramatically in this wavelength region, linear extrapolation of their data may not be valid. We considered using the $Cl + H_2CO \rightarrow HCO + HCl$ reaction to calibrate absolute HCO concentration. However, we did not use this calibration scheme since H_2CO photolysis would also have led to the formation of HCO.

The dependence of the HCO radical yield on *n*-pentanal pressure was examined. The HCO radical yield was found to be independent of *n*-pentanal pressure when photolysis was conducted in the wavelength range 280−325 nm. At 330-nm photolysis, the HCO radical yield decreased by ~25% when the *n*-pentanal pressure was increased from 2 to 18 Torr. Since the size of the HCO signal was small at 330 nm, it is unclear whether this decrease in the HCO yield was just the experimental error limit or it is due to dissociation at a near-threshold wavelength. The photolysis laser pulse energy was repeatedly monitored during the course of the HCO yield measurements so that any drop in photolysis photon energy with time was corrected. Also, the HCO yield at a given *n*-pentanal pressure was repeatedly measured during the course of the experiments in order to ensure the consistency of the results. HCO radical yields as a function of the photolysis wavelength thus obtained

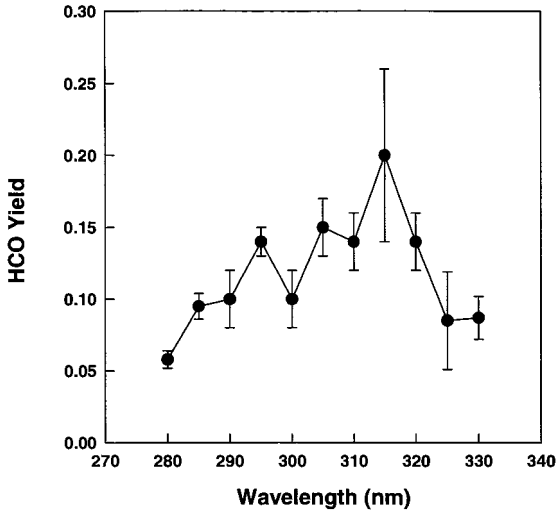

Figure 4. HCO quantum yield as a function of the *n*-pentanal photolysis wavelength.

are plotted in Figure 4 and listed in Table 1. Errors quoted reflect experimental scatter (1σ) which are estimated on the basis of at least two experimental runs consisting of about 8 aldehyde pressures per run. Systematic errors in the yield measurements include uncertainties in the determination of the following parameters: H_2CO concentration and absorption cross section (~24%), *n*-pentanal absorption cross section (5% in the 280−325-nm region; 16% at 330 nm), pulse energy (5%), and dye laser width. To estimate the effect of uncertainty in the determination of dye laser width on the absolute value of HCO yield, we calculated the HCO yield using a photolysis beam width of 0.15 and 0.20 cm. We found that HCO yield only differed by a maximum of 5% when the beam width varied from 0.15 to 0.20 cm. The presence of 1% *n*-pentanoic acid in *n*-pentanal will systematically lower the value of HCO yield by 1%. Photolysis of *n*-butyraldehyde also leads to the formation of HCO. An HCO yield of 0.34 was reported at 313 nm.[28,29] Assuming the HCO channel has a quantum yield of 0.34 in the 280−330-nm region, the presence of 0.07% *n*-butyraldehyde will lead to a maximum estimated uncertainty of 0.4% in HCO yield. The overall uncertainties of HCO yield measurements including both systematic error and experimental scatter are ~50% at 280, 285, and 295 nm; ~55% at 305, 310, and 320 nm; ~60% at 290 and 300 nm; 68% at 330 nm; 70% at 315 nm; 80% at 325 nm. As seen from Figure 4, the HCO yields increased to a maximum in the vicinity of 315 nm and then decreased at both longer and shorter wavelength ends. The decrease in HCO yields at higher photolysis photon energies can possibly be attributed to the opening up of additional *n*-pentanal photodissociation pathways (Product studies described later might also be suggestive of the $C_4H_{10} + CO$ channel at higher photolysis photon energies). The reduced HCO yields at the longer wavelength tail may be the result of photodissociation at a near-threshold wavelength.

The dependence of HCO radical yields on total pressure was examined by maintaining the constant *n*-pentanal pressure and varying the nitrogen carrier gas pressure. HCO radical yields were found to be independent of the total pressure when the total pressure was varied between 8 and 480 Torr with photolysis wavelengths shorter than 325 nm.

One might wonder if the HCO radical yield is dependent on *n*-pentanal pressure when *n*-pentanal pressure is on the order of hundreds of mTorr and if quenching of excited *n*-pentanal below its dissociation threshold has already occurred at the

n-pentanal pressures we worked with. To answer this question, we used a 308-nm excimer laser to photolyze *n*-pentanal. The much higher photon fluence from the excimer laser (~0.032 J/cm^2) and the larger overlapping distance between the photolysis and the probe lasers (4.6 cm) allowed us to determine the HCO yield as a function of *n*-pentanal pressure over 2 orders of magnitude of *n*-pentanal pressure. *n*-Pentanal pressures of 0.1, 0.2, 0.5, 1, 1.5, 2, 3, 4, 6, 8, and 10 Torr were used. The photolysis/probe laser delay was set at 5 μs. The HCO yield was found to be independent of *n*-pentanal pressure in the 0.1−4-Torr range. The HCO yield was about 15% lower from the photolysis of 10-Torr *n*-pentanal than that from 0.1 Torr. If HCO + HCO, HCO + C_4H_9, and C_4H_9 + C_4H_9 reactions at 5 μs after photolysis of 10-Torr *n*-pentanal were corrected for ($[HCO]_0 = [C_4H_9]_0 = 8.3 \times 10^{13}$ cm^{-3}), this difference amounts to only 8% over a 100-fold change in *n*-pentanal pressure. Also, the size of the HCO yield at 308 nm (~0.13) compared with those at 305 and 310 nm does not support the occurrence of significant quenching.

Analysis of End Products from the Photolysis of *n*-Pentanal. End products from the photolysis of *n*-pentanal/N_2 and *n*-pentanal/O_2 mixtures in a closed cell with ~15000 laser shots were analyzed by GC/MS and HPLC. HPLC was used to probe aldehyde products. GC/MS was employed to monitor nonpolar products. Limited use of analytical apparatus (GC/MS and HPLC) outside of our laboratory represented our best current effort to make quasi-steady-state end-product determinations. One major technical problem was that *n*-pentanal is sticky, making it difficult to transfer *n*-pentanal quantitatively from one vessel to another. We found that when we added the same *n*-pentanal pressure into a 25-mm × 36-cm cylindrical Pyrex cell, and then transferred the unphotolyzed sample to an HPLC cartridge or to a GC/MS sampling canister, the GC/MS and HPLC analysis did not show the same absolute response. Product studies therefore were qualitative. *n*-Pentanal, oxygen, and nitrogen pressures of 10, 160, and 160 Torr, respectively, were used in the experiments. Acetaldehyde was observed by HPLC after photolysis of an *n*-pentanal/N_2 mixture. This suggests the photofragmentation channel:

$$CH_3(CH_2)_3CHO + h\nu \rightarrow CH_3CH{=}CH_2 + CH_3CHO \quad (4)$$

Estimates of the quantum yields of aldehydes formed from the photolysis of an *n*-pentanal/N_2 mixture can be derived in the following manner. Total carbonyls are expected to be conserved before and after the photolysis of an *n*-pentanal/N_2 mixture. Assuming all the carbonyl groups from the photolysis of an *n*-pentanal/N_2 mixture existed as aldehydes and were detected by HPLC, then the fraction of individual aldehyde on the chromatogram can be estimated by summing up the peak areas of all the aldehydes and dividing the individual aldehyde peak area by the sum. The relative amount of individual aldehyde formed was equal to the difference in the ratio of the aldehyde peak area to the total peak area before and after photolysis. The relative amount of *n*-pentanal photolyzed was equal to the difference in the ratio of *n*-pentanal over the total peak area before and after photolysis. The estimated individual aldehyde yield was obtained by dividing the amount of aldehyde formed by the amount of *n*-pentanal photolyzed. Since carbonyl groups from the photolysis of an *n*-pentanal/N_2 mixture may also exist as CO, and it was not detected by HPLC, the analysis mentioned above only provided a crude estimate of aldehyde yields. The acetaldehyde quantum yields thus obtained are ~84%, 91%, and 68% at 290, 310, and 330 nm, which are also listed in Table 2. When an *n*-pentanal/O_2 mixture was photolyzed, secondary oxidation products such as *n*-butyraldehyde, propionaldehyde, acetone, and formaldehyde were also detected by HPLC. More *n*-pentanal was consumed when an *n*-pentanal/O_2 mixture was photolyzed compared to that of an *n*-pentanal/N_2 mixture. Also, the relative product distributions were changed. On one hand, relative product ratios from photolysis of an *n*-pentanal/O_2 mixture at 290, 310, and 330 nm are acetaldehyde/propionaldehyde ~ 1, 0.15, and 0.054, respectively; acetaldehyde/acetone ~ 1, 0.0043, and 0.005, respectively; acetaldehyde/H_2CO ~ 1, 0.030, and 0.22, respectively; acetaldehyde/*n*-butyraldehyde ~ 1, 0.32, and 0.065, respectively. On the other hand, acetaldehyde/*n*-butyraldehyde ratios of 1, 1.6, and 0.34 at 290, 310, and 330 nm were obtained from *n*-pentanal/N_2 photolysis.

TABLE 2: Products from Closed-Cell Photolysis of *n*-Pentanal at Several Wavelengths

sample	photolysis wavelength	products observed and yields[a] GC/MS	HPLC
n-pentanal/N_2	290 nm	1-butene 1-propene butane *n*-octane	CH_3CHO (84%) H_2CO (2.5%) $CH_3(CH_2)_2CHO$ (12%)
	310 nm		CH_3CHO (91%) H_2CO (2.4%) $CH_3(CH_2)_2CHO$ (6.8%)
	330 nm	1-butene 1-propene	CH_3CHO (68%) H_2CO (1.1%) $CH_3(CH_2)_2CHO$ (28%)
n-pentanal/O_2	290 nm	1-butene 1-propene butane	CH_3CHO H_2CO CH_3CH_2CHO CH_3COCH_3 $CH_3(CH_2)_2CHO$
	310 nm		CH_3CHO H_2CO CH_3CH_2CHO CH_3COCH_3 $CH_3(CH_2)_2CHO$
	330 nm	1-butene 1-propene	CH_3CHO H_2CO CH_3CH_2CHO CH_3COCH_3 $CH_3(CH_2)_2CHO$

[a] Yields were estimated assuming that total carbonyls were conserved before and after photolysis of an *n*-pentanal/N_2 mixture. *n*-Pentanal photolyzed was generally less than 10%.

GC/MS detection of photolysis products suggested the existence of several product channels leading to the formation of alkenes and alkanes. For instance, photolysis of an *n*-pentanal/N_2 mixture at 330 nm led to the formation of 1-propene and 1-butene. 1-Propene can be generated from the acetaldehyde channel (see eq 4). 1-Butene may be produced from the following channel:

$$CH_3(CH_2)_3CHO + h\nu \rightarrow CH_3CH_2CH{=}CH_2 + H_2CO \quad (8)$$

At 290 nm, the photolysis of an *n*-pentanal/N_2 mixture led to the formation of additional products such as butane and *n*-octane. Butane is possibly a product of the following photodissociation channel:

$$CH_3(CH_2)_3CHO + h\nu \rightarrow C_4H_{10} + CO \quad (1)$$

The observation of butane at the shorter photodissociation wavelength is consistent with results from the wavelength-dependent HCO yield measurements which could be suggestive of additional photolysis pathways at higher photon energies.

Because of the overlapping GC/MS peaks of *n*-butane and other products, we could not extract an *n*-butane yield from the 290-nm photolysis of an *n*-pentanal/N_2 mixture. *n*-Octane can be formed from the recombination of C_4H_9:

$$C_4H_9 + C_4H_9 \rightarrow C_8H_{18} \quad (9)$$

In the presence of oxygen, *n*-octane disappeared possibly due to the formation of butyl peroxy radicals ($C_4H_9O_2$):

$$C_4H_9 + O_2 \rightarrow C_4H_9O_2 \quad (10)$$

A summary of the product study using GC/MS and HPLC is included in Table 2.

A previous study[24] on the photolysis of *n*-butyraldehyde at 308 nm indicated the yield of ethylene (a coproduct of the acetaldehyde channel) decreased by 45% when 500-Torr air was added to 20-Torr *n*-butyraldehyde. It would be very interesting to examine the dependence of the acetaldehyde yield as a function of the oxygen pressure and total pressure from *n*-pentanal photolysis.

Atmospheric Photodissociation Rate Constant To Form the HCO Radical. The photodissociation rate constant (k_{rad}) for *n*-pentanal to form the HCO radical (or HO_2 in the presence of air) was calculated from the actinic solar flux ($J(\lambda)$) reported by Demerjian et al.,[30] the absorption cross section ($\sigma(\lambda)$) of *n*-pentanal and the HCO radical yield ($\Phi(\text{rad}, \lambda)$) from *n*-pentanal photolysis, both from the present study, using the relationship

$$k_{rad} = \int \sigma(\lambda)\Phi(\text{rad},\lambda)J(\lambda)\, d\lambda \quad (11)$$

The photolysis rate constants of *n*-pentanal to form HCO for noontime on January 1 and July 1 under cloudless conditions at sea level and a latitude of 40° N were calculated to be 5.0×10^{-6} and 1.6×10^{-5} s^{-1}, respectively. If both primary HCO yield from the photolysis of *n*-pentanal and secondary HCO yield from the photolysis of the acetaldehyde product were included by using literature acetaldehyde absorption cross section and quantum yield data,[26] calculated radical formation rate constants for noontime on January 1 and on July 1 are 6.9×10^{-6} and 2.5×10^{-5} s^{-1}, respectively. Acetaldehyde photodissociation rate constants that lead to radical formation are 2.6×10^{-6} s^{-1} for January 1 and 1.1×10^{-5} s^{-1} for July 1. The calculated radical formation rate constants from *n*-pentanal photolysis are 1.9−2.7 times and 1.5−2.3 times as fast as those obtained from acetaldehyde photolysis for January 1 and July 1 conditions, respectively (the lower limit in the range did not include the HCO radical formed from the photolysis of the acetaldehyde product; the upper limit assumed acetaldehyde yields from the photolysis of *n*-pentanal at atmospheric pressure were 0.84, 0.91, and 0.68 at 290, 310, and 330 nm, respectively (see Table 2)). Thus, the radical formation capability of longer chain aldehydes such as *n*-pentanal is significant.

Acknowledgment. We thank Mr. Andrew Levine for his assistance in the experiments and for calculating the photolysis rates. We are grateful to Dr. Xianliang Zhou, Ms. Guo Hong, Dr. Amarjit Narang, and Ms. Michele Losavio for performing HPLC analysis of photolysis products, and to Dr. Ken Aldous and Mr. Michael Force for GC/MS analysis of photodissociation products. Helpful discussions and suggestions by Professor Robert Keesee, Dr. Xianliang Zhou, Dr. Stephen Riley, and Dr. Geoffrey Tyndall are acknowledged. This work was supported by the National Science Foundation under Grant No. ATM-9610285.

References and Notes

(1) Graedel, T. E.; Farrow, L. A.; Weber, T. A. *Atmos. Environ.* **1976**, *10*, 1095.
(2) Grosjean, D. *Environ. Sci. Technol.* **1982**, *16*, 254.
(3) Finlayson-Pitts, B. J.; Pitts, J. N., Jr. *Atmospheric Chemistry*; John Wiley: New York, 1986.
(4) Moortgat, G. K.; Seiler, W.; Warneck, P. *J. Chem. Phys.* **1983**, *78*, 1185.
(5) Carmely, Y.; Horowitz, A. *Int. J. Chem. Kinet.* **1984**, *16*, 1585.
(6) Moore, C. B.; Weisshaar, J. C. *Annu. Rev. Phys. Chem.* **1983**, *34*, 525.
(7) Ho, P.; Bamford, D. J.; Buss, R. J.; Lee, Y. T.; Moore, C. B. *J. Chem. Phys.* **1982**, *76*, 3630.
(8) Horowitz, A.; Calvert, J. G. *J. Phys. Chem.* **1982**, *86*, 3105.
(9) Meyrahn, H.; Moortgat, G. K.; Warneck, P. Presented at the 15th Informal Conference on Photochemistry, Stanford, CA, July 1982.
(10) Shepson, P. B.; Heicklen, J. *J. Photochem.* **1982**, *19*, 215.
(11) Heicklen, J.; Desai, J.; Bahta, A.; Harper, C.; Simonaitis, R. *J. Photochem.* **1986**, *34*, 117.
(12) Terentis, A. C.; Knepp, P. T.; Kable, S. H. *J. Phys. Chem.* **1995**, *99*, 12704.
(13) Calvert, J. G.; Pitts, J. N., Jr. *Photochemistry*; John Wiley: New York, 1966.
(14) Lee, E. K. C.; Lewis, R. S. *Adv. Photochem.* **1980**, *12*, 1.
(15) O'Keefe, A.; Deacon, D. A. G. *Rev. Sci. Instrum.* **1988**, *59*, 2544.
(16) O'Keefe, A.; Scherer, J. J.; Cooksy, A. L.; Sheeks, R.; Heath, J.; Saykally, R. J. *Chem. Phys. Lett.* **1990**, *172*, 214.
(17) Zhu, L.; Johnston, G. *J. Phys. Chem.* **1995**, *99*, 15114.
(18) Zhu, L.; Kellis, D.; Ding, C.-F. *Chem. Phys. Lett.* **1996**, *257*, 487.
(19) Martinez, R. D.; Buitrago, A. A.; Howell, N. W.; Hearn, C. H.; Joens, J. A. *Atmos. Environ.* **1992**, *26A*, 785.
(20) Herzberg, G.; Ramsay, D. A. *Proc. R. Soc. (London)* **1955**, *A233*, 34.
(21) Johns, J. W. C.; Priddle, S. H.; Ramsay, D. A. *Discuss. Faraday Soc.* **1963**, *35*, 90.
(22) Stoeckel, F.; Schuh, M. D.; Goldstein, N.; Atkinson, G. H. *Chem. Phys.* **1985**, *95*, 135.
(23) Reilly, J. P.; Clark, J. H.; Moore, C. B.; Pimentel, G. C. *J. Chem. Phys.* **1978**, *69*, 4381.
(24) Baggott, J. E.; Frey, H. M.; Lightfoot, P. D.; Walsh, R. *J. Phys. Chem.* **1987**, *91*, 3386.
(25) Adach, H.; Basco, N. *Int. J. Chem. Kinet.* **1981**, *13*, 367.
(26) Atkinson, R.; Baulch, D. L.; Cox, R. A.; Hampson, R. F., Jr.; Kerr, J. A.; Troe, J. *J. Phys. Chem. Ref. Data*, **1992**, *21*, 1125.
(27) Cantrell, C. A.; Davidson, J. A.; McDaniel, A. H.; Shetter, R. E.; Calvert, J. G. *J. Phys. Chem.* **1990**, *94*, 3902.
(28) Förgeteg, S.; Bérces, T.; Dóbé, S. *Int. J. Chem. Kinet.* **1979**, *11*, 219.
(29) Blacet, F. E.; Calvert, J. G. *J. Am. Chem. Soc.* **1951**, *73*, 667.
(30) Demerjian, K. L.; Schere, K. L.; Peterson, J. T. *Adv. Environ. Sci. Technol.* **1980**, *10*, 369.